Organic Electronics Hot Paper

How to cite: *Angew. Chem. Int. Ed.* **2022,** *61,* e202207204
International Edition: doi.org/10.1002/anie.202207204
German Edition: doi.org/10.1002/ange.202207204

Pure Hydrocarbon Materials as Highly Efficient Host for White Phosphorescent Organic Light-Emitting Diodes: A New Molecular Design Approach

Fan-Cheng Kong[+], Yuan-Lan Zhang[+], Cassandre Quinton[+], Nemo McIntosh[+], Sheng-Yi Yang, Joëlle Rault-Berthelot, Fabien Lucas, Clément Brouillac, Olivier Jeannin, Jérôme Cornil, Zuo-Quan Jiang, Liang-Sheng Liao,* and Cyril Poriel**

Abstract: To date, all efficient host materials reported for phosphorescent OLEDs (PhOLEDs) are constructed with heteroatoms, which have a crucial role in the device performance. However, it has been shown in recent years that the heteroatoms not only increase the design complexity but can also be involved in the instability of the PhOLED, which is nowadays the most important obstacle to overcome. Herein, we design pure aromatic hydrocarbon materials (PHC) as very efficient hosts in high-performance white and blue PhOLEDs. With EQE of 27.7 %, the PHC-based white PhOLEDs display similar efficiency as the best reported with heteroatom-based hosts. Incorporated as a host in a blue PhOLED, which are still the weakest links of the technology, a very high EQE of 25.6 % is reached, surpassing, for the first time, the barrier of 25 % for a PHC and FIrpic blue emitter. This performance shows that the PHC strategy represents an effective alternative for the future development of the OLED industry.

Introduction

Organic optoelectronics has experienced a fantastic development over the last twenty years thanks to the great progress made in the emerging technologies of Organic Light-Emitting Diodes (OLEDs).[1] Three main families of emitting materials based on different photophysical concepts have been developed to date: fluorescence (generation I),[2–4] phosphorescence (generation II),[5–11] and thermally-activated delayed fluorescence (TADF, generation III).[12–14] From a technological point of view, generation II is the most mature and now released on the market. However, there is room for improvement as this technology is still far from reaching its full potential in daily life. Of particular interest, the design of new generations of host materials free from heteroatoms (called PHC for Pure HydroCarbons) has aroused ongoing interest in recent years to improve the stability of phosphorescent OLEDs (PhOLEDs).[10,15–22] Indeed, it is recognized that the OLED instability, which is the main problem to address at the current stage of development, is partially caused by the fragile C–N, C–P and C–S bonds involving heteroatoms in host compounds.[23–25] To gain insights into the instability of PhOLEDs, the chemical stabilities of various molecular fragments (such as the widely known electron-accepting aryl phosphine oxide fragment) in their first triplet excited state (T_1) have recently been studied.[26] It has been shown that the phosphorus–carbon bonds of aryl phosphoryl fragments are significantly more vulnerable to dissociation in their T_1 states than in their ground (S_0) states. Removing the heteroatoms from the molecular backbone of the host has also beneficial consequences on the synthetic complexity and production cost, contributing to simplifying the technology, which is nowadays a key feature for the ecological transition.[9] However, switching from heteroatom-based hosts to PHC hosts has dramatic impacts on the efficiency of the devices, notably due to the inherently low charge carrier mobilities of the PHC materials. Thus, in spite of a longstanding concept introduced for the first time in 2005,[15] the PHC strategy has attracted little attention over the last 15 years owing to the

[*] F.-C. Kong,[+] Y.-L. Zhang,[+] S.-Y. Yang, Z.-Q. Jiang, L.-S. Liao
Institute of Functional Nano & Soft Materials (FUNSOM), Jiangsu Key Laboratory for Carbon-Based Functional Materials & Devices, Soochow University
Suzhou, Jiangsu 215123 (China)
E-mail: zqjiang@suda.edu.cn
lsliao@suda.edu.cn

C. Quinton,[+] J. Rault-Berthelot, F. Lucas, C. Brouillac, O. Jeannin, C. Poriel
Univ. Rennes, CNRS, ISCR-UMR 6226
35000 Rennes (France)
E-mail: Cyril.poriel@univ-rennes1.fr

N. McIntosh,[+] J. Cornil
Laboratory for Chemistry of Novel Materials,
University of Mons
7000 Mons (Belgium)

L.-S. Liao
Macau Institute of Materials Science and Engineering,
Macau University of Science and Technology
Macao, 999078 (China)

[+] These authors contributed equally to this work.

difficulty to design highly efficient host materials. The situation has now changed. In 2019, our groups have proposed that the C1 site of the 9,9′-spirobifluorene (SBF) scaffold was critical for constructing a new generation of PHC hosts leading to the first series of high-performance PHC-based PhOLEDs.[17] Very high EQE up to 23 % was obtained in blue PhOLEDs, which are the most challenging to reach.[2,11,27] Despite this encouraging progress, the performance was still incomparable with those reported for the best heteroatom-based hosts.[28–34] In 2020, this barrier was lifted and a PHC material surpassed the performance of heteroatom-based materials as a universal host in Red, Green, and Blue (RGB) PhOLEDs.[10] Reaching the grail of the OLED technology, namely the white-emitting PhOLED, with PHC hosts is now the next challenge to take up. In this work, we use the C1-site of the SBF scaffold to design very high efficiency PHC hosts for white light emission. Despite the fact that the SBF fragment is one of the most efficient scaffolds used in organic electronics,[2,8,35–41] its substitution at C1 is almost absent from the literature and has only been reported very recently.[17,42,43] The C1 site forms a *meta* linkage with the bridged biphenyl (i.e. fluorene) unit, leading in principle to an electronic decoupling between the two fragments. In addition, oppositely to the C3 site (also forming a *meta* linkage), the C1 site is highly sterically hindered due to the presence of the cofacial fluorene. These two characteristics (i.e. *meta* linkage and high steric hindrance) avoid an extended conjugation pathway, which would lead to a decrease of S_1/T_1 and energy back-transfers from the guest to the host, reducing in turn the PhOLED efficiency. Given that the substituent itself has also a crucial role in the device performance, three different side groups were investigated in this work: phenyl for 1-p-SBF, *meta*-biphenyl for 1-mbp-SBF and *meta*-terphenyl for 1-mtp-SBF (see molecular structures in Figure 1a). These side groups strongly influence not only the thermal properties but also the charge transport properties dictating the PhOLED performance.

The *meta*-terphenyl derivative 1-mtp-SBF achieves a high first singlet–triplet state energy (E_{S1}/E_{T1}) of 3.96/2.88 eV and yields an impressive external quantum efficiency (EQE) of 27.7 % in white PhOLEDs using a simple single emissive layer (EML), constructed with sky-blue (FIrpic, Bis[2-(4,6-difluorophenyl)pyridinato-C2,N](picolinato)iridium(III)) and yellow phosphorescent (PO-01, bis(4-phenylthieno[3,2-c]pyridinato-N,C2′)(acetylacetonate)iridium(III)) emitters. This PHC-based single-layer white PhOLED displays similar efficiency to the best reported to date with heteroatom-based hosts, bridging definitively the gap between heteroatom-based and PHC hosts.[33,44–53] In addition, 1-mtp-SBF incorporated as a host in blue PhOLEDs, which are still the weakest link of the RGB OLED technology,[2,11,27] displays an excellent EQE of 25.6 %, surpassing, for the first time, the barrier of 25 % with a PHC hosting FIrpic as the blue emitter. This performance shows that the PHC design strategy represents an effective alternative for the future development of OLED technology as a high-performance and very simple low-cost option.

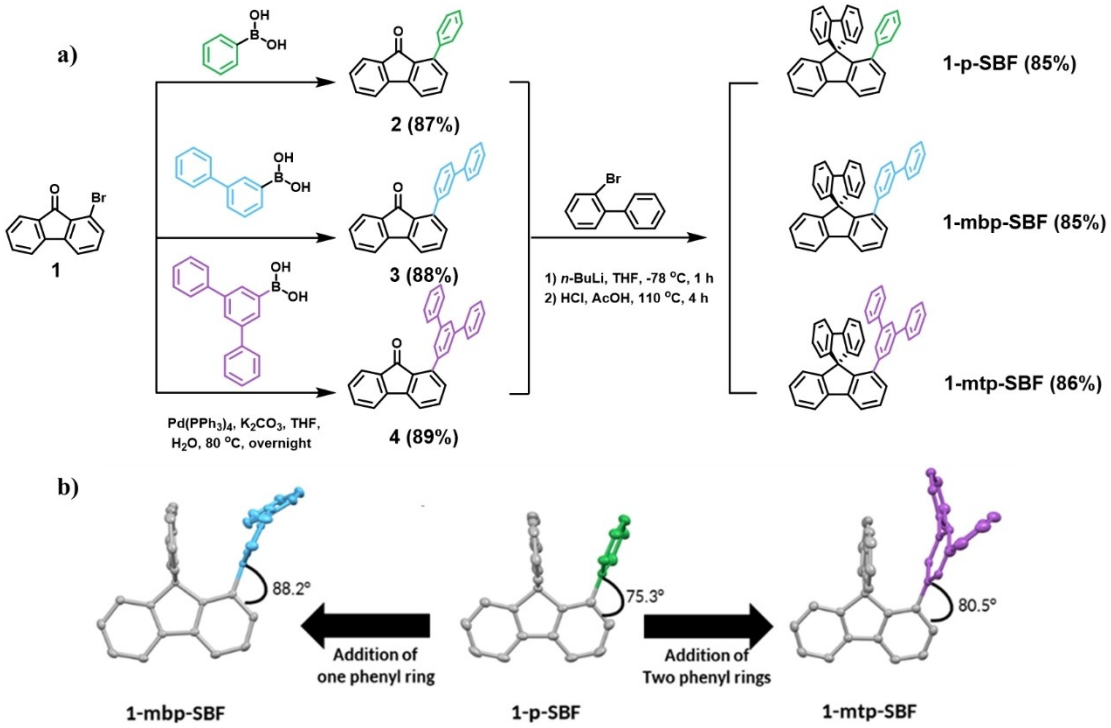

Figure 1. a) Synthesis of PHC hosts. b) Dihedral angle variation when adding a benzene ring (ORTEP at the 50 % of probability level, hydrogen, and solvent molecules hidden).

Table 1: Selected electronic and physical properties.

		1-p-SBF	1-mbp-SBF	1-mtp-SBF	SBF[43]
λ_{Abs} (ε).[a] [nm] (10^4 L mol^{-1} cm^{-1})		298 (0.98) 309 (1.66)	299 (0.96) 310 (1.57)	299 (0.96) 310 (1.39)	297 (0.72) 308 (1.45)
λ_{EM}[a] [nm]		313, 323	311, 323	313, 328	310, 323
k_r [ns^{-1}][a]		0.117	0.081	0.016	0.120
k_{nr} [ns^{-1}][a]		0.075	0.108	0.096	0.100
ϕ[a]		0.61	0.43	0.14	0.55
E_{S1}[b] [eV]		3.99	3.97	3.96	4.05
E_{T1} [eV]	Opt.[c]	2.88	2.88	2.88	2.89
	Calc.[d]	2.65	2.67	2.67	–
τ_p (s)[c]		5.6	5.5	5.6	5.4
τ_f [ns][a]		5.2	5.3	9.0	4.6
E_g [eV]	Opt.[e]	3.95	3.93	3.92	3.97
	Elec.[f]	4.13	4.08	4.05	4.16
LUMO [eV] (E_{onset}^{red} [V])	Elec.[g]	- 1.81 (- 2.59)	- 1.85 (- 2.55)	- 1.88 (- 2.52)	- 1.81[j] (- 2.59)
	Calc.[d]	-1.28	-1.33	-1.36	- 1.26
HOMO [eV] (E_{onset}^{ox} [V])	Elec.[g]	- 5.94 (1.54)	- 5.93 (1.53)	- 5.93 (1.53)	- 5.97[j] (1.57)
	Calc.[d]	-5.96	-5.98	-5.96	-5.99
Thermal [°C]	T_g	49	66	90	–
	T_d	272	384	387	234[17]
Mobility [cm^2 V^{-1} s^{-1}]	μ_h (10^{-6})[h]	0.64	8.80	33.52	–
	μ_e (10^{-6})[i]	0.42	2.06	16.79	–

[a] In cyclohexane at room temperature. [b] Calculated from the onset of the lowest energy band in cyclohexane (1239.84/λ). [c] Calculated from the peak maximum of the lowest phosphorescent band, (1239.84/λ), at 77 K in 2-MeTHF. [d] From TD-DFT calculations (B3LYP/6-311+g(d,p)). [e] Calculated from the onset of the UV/Vis absorption spectrum in cyclohexane. [f] Calculated from |HOMO (CH_2Cl_2)-LUMO (DMF)|. [g] From CVs (CH_2Cl_2 in oxidation and DMF in reduction). [h] Hole mobility (μ_h). [i] Electron mobility (μ_e). [j] The HOMO/LUMO values of SBF measured in this work are slightly different from those previously reported (HOMO/LUMO: −5.95/−1.74 eV).[43]

Results and Discussion

The synthetic approach developed is short with high yields and has allowed to easily synthesize the three compounds at the multi-gram scale (Figure 1a). This is a key feature for further industrialization. Pendant substituents, phenyl, biphenyl, and terphenyl were first attached at the C1 site of 1-bromofluorenone 1[54] by Pd-catalysed coupling providing fluorenones 2–4. Then, incorporation of the spirofluorene fragment via a classical sequence (nucleophilic addition with 2-LiPh_2 and intramolecular aromatic electrophilic substitution of the resulting fluorenols) gives the targeted compounds with high yields over 85 %.

One of the particularities of C1-based SBFs, which in turn drives the electronic properties, is the high dihedral angle measured between the substituent attached at C1 and the fluorene. This angle governs the degree of π-conjugation extension. In the present case, the crystal structures confirm the strong steric congestion of these structures with high dihedral angles of 66.6/75.3° for 1-p-SBF (2 molecules are present in the asymmetric unit), 88.2° for 1-mbp-SBF and 80.5° for 1-mtp-SBF, respectively (Figure 1b).[55] This structural particularity is induced by the substitution at *ortho*-position of the spiro carbon, which provides a sterically hindered environment due to the presence of the cofacial fluorene. This is corroborated by the short C–C distances detected between carbon atoms of the non-substituted fluorene and those of the cofacial phenyl ring. These structural features highlight the importance of steric parameters in the electronic properties presented below.

All the hosts display almost identical UV/Vis absorption profiles (Figure 2a). In cyclohexane, the spectra are well structured with thin and high-intensity bands at 298–299 nm and 309–310 nm. These spectra are almost identical to that of the building unit SBF,[43] implying that the substituent attached at C1 has very little influence on the absorption properties. Indeed, the four transitions corresponding to these two bands in these systems are fully driven by the fluorene cores with no involvement of the substituent, as shown by TD-DFT (Figure 2b and Figure S1–S3). This shows that the C1 site effectively breaks the conjugation between the fluorene and its substituent due to the joint

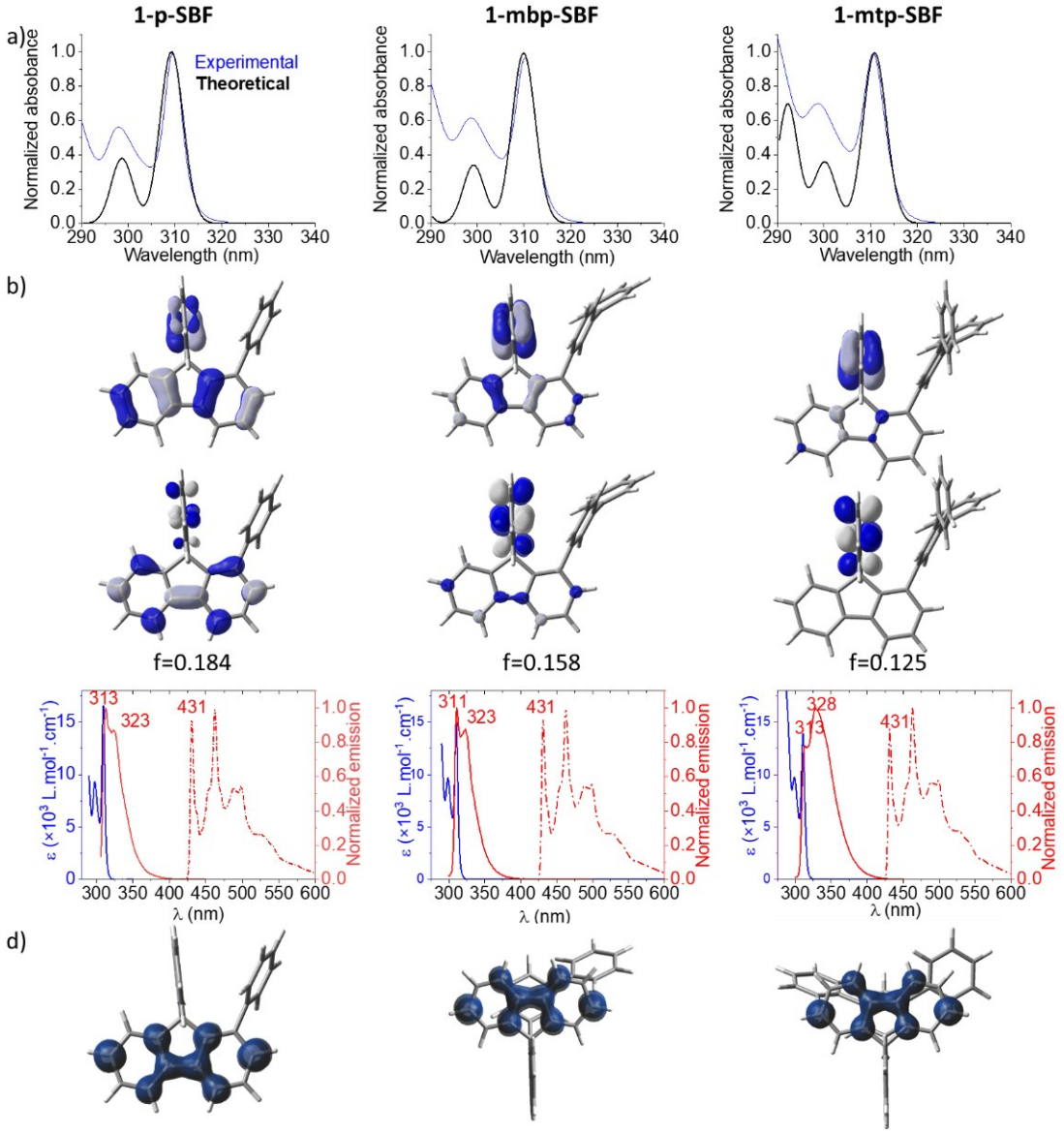

Figure 2. a) Normalized experimental absorption spectra in cyclohexane and TD-DFT (M06-2X, 6-311+g(d,p)) simulated spectra. b) Natural transition orbital pairs ("hole" on the top and "electron" on the bottom) for the first singlet excited state S_1 and the oscillator strength associated to $S_0 \rightarrow S_1$ transition obtained by TD-DFT (M06-2X, 6-311+g(d,p), isovalue of 0.04). c) Absorbance in cyclohexane at RT, fluorescence in cyclohexane at RT and phosphorescence in 2-methyltetrahydrofuran at 77 K. d) Triplet spin density distribution (TD-DFT, B3LYP, 6-311+g(d,p), isovalue of 0.004) of 1-p-SBF (left), 1-mbp-SBF (middle) and 1-mtp-SBF (right), respectively.

effect of steric hindrance and *meta* linkage. This characteristic appears to be unique in the family of SBF positional isomers,[37] while the C3[10] or C4[8,56] position previously described in literature only provides partial conjugation breaking. The optical gaps (E_g, determined from the onset of the absorption spectra in cyclohexane) of 1-p-SBF, 1-mbp-SBF, and 1-mtp-SBF are estimated at 3.95, 3.93, and 3.92 eV, respectively, which are compatible with their use as hosts in PhOLEDs. The phosphorescence emission spectra, recorded at 77 K in 2-MeTHF (Figure 2c), provide the corresponding E_{T1} of 1-p-SBF, 1-mbp-SBF and 1-mtp-SBF, estimated at 2.88 eV ($\lambda_{max}=431$ nm). For all compounds, the emission from the T_1 state is confirmed by the very long lifetime measured ($\tau=5.5$–5.6 s, Table 1). It is worth noting that E_{T1} of the three compounds are found to be identical as a result of the efficient confinement of triplet excitons on one fluorene. Since E_{T1} of SBF is measured at 2.89 eV in 2-MeTHF,[43] these data clearly show that the nature of the substituent (phenyl, biphenyl, and terphenyl) grafted at C1 of a SBF scaffold does not influence E_{T1}.[43] The spin density is indeed spread out on one fluorene, the substituted one in 1-p-SBF and the unsubstituted one in 1-mbp-SBF and 1-mtp-SBF, with no involvement of the substituent (Figure 2d). It should be noted that theoretical calculations provide similar E_{T1} for the three compounds, following the experimental results (Table 1). However, the nature of

substituents has a remarkable impact on other properties such as thermal properties and mobility of charge carriers as detailed below. This control of the electronic properties is a key step for materials design.

E_g and E_{T1} are thus independent of the nature of the substituents, the peripheral phenyl rings of both 1-mbp-SBF and 1-mtp-SBF having a negligible effect on these parameters. However, in fluorescence, the peripheral rings impact the vibrational relaxation of molecules in their excited states. This leads to a weak red shift of the emission bands in the case of 1-mtp-SBF (λ_{max} = 313/328 nm) compared with both 1-p-SBF (λ_{max} = 313/323 nm) and 1-mbp-SBF (λ_{max} = 311/323 nm). This is due to a partial planarization of the terphenyl backbone in the first excited state, which increases the delocalization. This shows that adding peripheral rings on the substituents as in 1-mtp-SBF can modify the fluorescence spectra while keeping identical absorption and phosphorescence spectra. Interestingly, the quantum yield of these PHCs decreases as the size of substituent increases: 0.61 for 1-p-SBF, 0.43 for 1-mbp-SBF, and 0.14 for 1-mtp-SBF, respectively. This feature can be correlated to a consistent decrease in the radiative constant k_r (0.117, 0.081 and 0.016 ns^{-1} respectively), in accordance with a decrease in the oscillator strength for the $S_0 \rightarrow S_1$ transition (0.184, 0.158 and 0.125 respectively) and decrease of the delocalization (Natural Transitions Orbitals are localized on both fluorenes in 1-p-SBF and mainly on the unsubstituted fluorene in 1-mbp-SBF and 1-mtp-SBF, Figure 2b). In addition, the non-radiative constant k_{nr} remains similar (0.075, 0.108 and 0.096 ns^{-1} respectively), despite the addition of phenyl units which should increase the molecular motions (Table 1). In order to confirm the influence of the size of the substituent, which is herein a key point, we have attached a quaterphenyl fragment with four *meta* linkages on the SBF scaffold (called 1-mqp-SBF, see Supporting Information). As we expect, the quantum yield continues to decrease (from 0.14 for 1-mtp-SBF to 0.12 for 1-mqp-SBF) while the lifetime significantly increases (from 9.0 to 15.7 ns from 1-mtp-SBF to 1-mqp-SBF). The trend highlighted above is followed as k_r continues to dramatically dropdown (from 0.016 to 0.0076 ns^{-1} from 1-mtp-SBF to 1-mqp-SBF). Note that the 1-mqp-SBF model compound presents a fluorescence spectrum significantly red-shifted (λ_{max} = 348 nm, Figure S11) compared to 1-p-SBF (323 nm), 1-mbp-SBF (323 nm), and 1-mtp-SBF (328 nm), confirming that the S_1 state energy can be decreased when tuning the size of the substituent.

The electrochemical properties were analyzed by cyclic voltammetry (CV) in CH_2Cl_2 (oxidation) and DMF (reduction) and compared with those of the constituting units: SBF, biphenyl BP, and *m*-terphenyl *m*TP (Figure 3 and Figures S28 and S29). The three C1-substituted-SBFs are oxidized in two successive oxidation waves (Figure S28c), the first one being irreversible (Figure 3a) and very close to that of its building unit SBF (see E_{onset}^{ox} in Table 1). When reaching the second oxidation, electrodeposition processes

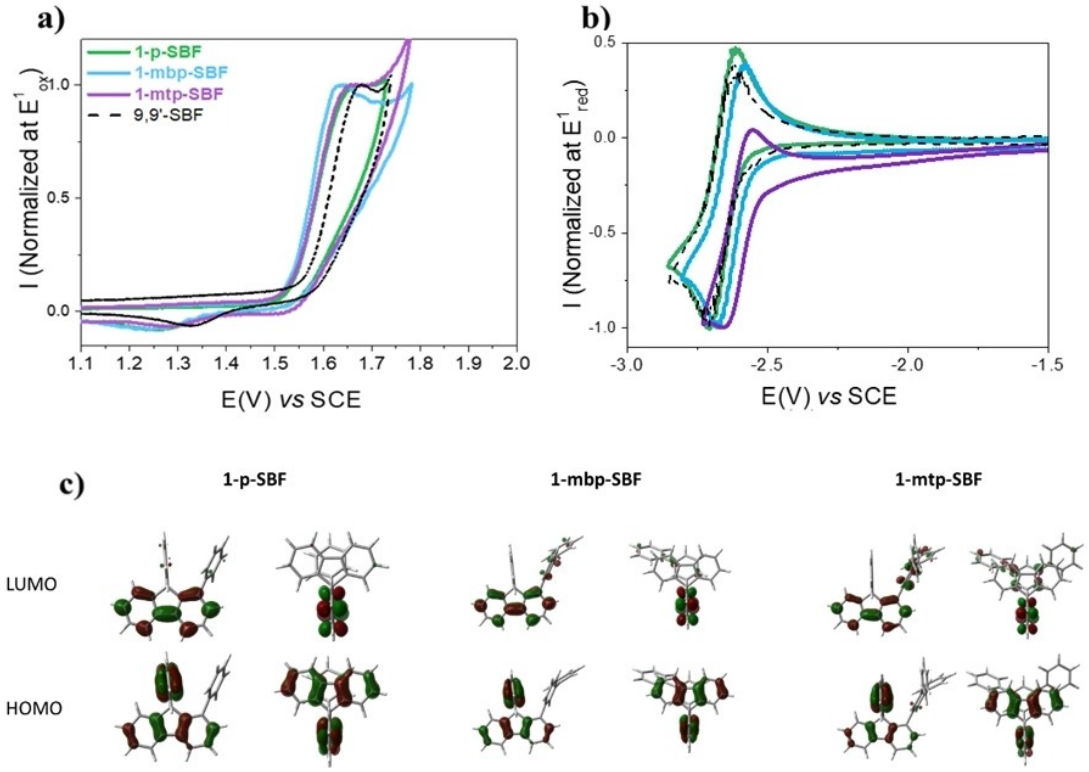

Figure 3. a) The cyclic voltammetry (CV) data of 1-p-SBF, 1-mbp-SBF and 1-mtp-SBF compared to SBF (a/In oxidation: CH_2Cl_2/[Bu_4NPF_6] 0.2 M, b/In reduction: DMF/[NBu_4PF_6] 0.1 M; sweep rate of 100 mV^{-1}, platinum disk working electrode). b) Frontier molecular orbitals (top: LUMO, bottom: HOMO, M06-2X, 6-311 + g(d,p), isovalue of 0.04).

are evidenced by: i) a reduction wave at the reverse scan and ii) the coverage of the platinum electrode surface by insoluble deposits. These electrodeposition processes occurring at the position C2/C7 of the fluorene are well known for SBF-based compounds,[57,58] Figures S30, S32 and S34. The HOMO levels were measured at −5.94 eV for 1-p-SBF and at −5.93 eV for both 1-mbp-SBF and 1-mtp-SBF, which are almost identical to that of SBF (−5.97 eV). This shows that the effect of the substituent is almost entirely erased upon substitution at the C1 site, highlighting the efficiency of the molecular design strategy. It is important to note that the HOMOs of the corresponding building blocks, BP and *m*TP, are significantly lower (−6.13 and −6.05 eV respectively, Figure S3 –S40). This is due to the different distribution of the HOMO, which is spread out on the fluorene backbones in all C1-SBF substituted compounds and not on the substituents (Figure 3c).

The cathodic explorations provide a different result. In DMF, all compounds present two successive reduction waves and are reduced in a larger potential range (Figure S29c). The first reduction wave is reversible (Figure 3b) with a peak maximum recorded at −2.71 V for 1-p-SBF, −2.68 V for 1-mbp-SBF and −2.66 V for 1-mtp-SBF, respectively. Compared to the first reduction of SBF (−2.71 V), 1-p-SBF is reduced at the same potential whereas the two others are reduced before SBF. Recently, in structurally related molecular systems, the impact of the nature of the phenyl linkages and the steric congestion, which are the two main parameters driving the electronic properties of organic semiconductors, has been unravelled.[43] It has been notably shown that these two parameters have a different impact as a function of the frontier molecular orbital considered, i.e. HOMO (benzenoidal) or LUMO (quinoidal). In addition, it has been shown that the torsions (steric effect) have a larger influence on the HOMO energy than on the LUMO energy, the latter being more sensitive to the electronic effect of the linkage. The present results widen the range of molecular systems following these design rules. Indeed, molecular modelling shows that the HOMO distributions of 1-p-SBF, 1-mbp-SBF and 1-mtp-SBF are almost identical, in full consistency with the fact that the HOMO energy levels determined by electrochemistry are identical as well. This is due to the high dihedral angle, imposed by the C1 position, between the fluorene and the pending substituents (Figure 1b). Oppositely, the LUMO appears to be less affected by the steric congestion and clearly shows an increasing contribution of the pending substituent when the size of the substituent increases. This is experimentally confirmed by the decrease in the LUMO energy level −1.81 eV for 1-p-SBF, −1.85 eV for 1-mbp-SBF and −1.88 eV for 1-mtp-SBF, respectively. Another effect is that the C1 site has a node in the HOMO wavefunction and a finite electronic density in the LUMO, thus further rationalizing that the HOMO energy level is less affected by substitution. The model compound 1-mqp-SBF also confirms this trend with an even lower LUMO energy level found at −1.98 eV (Figure S41), and a significant implication of the tetraphenyl core in the LUMO distribution. It should be mentioned that the LUMO of the building units *m*TP is lower than that of BP (−1.90 vs −1.80 eV, Figures S37 and S39), highlighting the effect of the extension of the conjugation despite the presence of a *meta*-linkage. Thus, the HOMO/LUMO gaps (E_g) of 1-mbp-SBF (4.08 eV), 1-mtp-SBF (4.05 eV), and 1-p-SBF (4.13 eV) are very large, which is a key feature to nest the phosphor in the emissive layer of the PhOLED (see below). One can nevertheless note a gap contraction compared to that of SBF (4.16 eV) by selectively reducing the LUMO level energy.

One of the strengths of PHCs constructed on the SBF scaffold is the thermal and morphological stability, which is a crucial point for OLED stability. All PHCs investigated herein display excellent thermal stability measured via thermogravimetric analysis (TGA). The high decomposition temperatures at 5 % mass loss (T_d) of 1-p-SBF, 1-mbp-SBF, and 1-mtp-SBF are 272, 384, and 387 °C, respectively, guaranteeing the stability of molecules under vacuum evaporation (Figure S42). Moreover, the glass transition temperatures T_g (determined by differential scanning calorimetry) increase with the size of the substituent reaching 90 °C in the case of 1-mtp-SBF (Table 1).

Before investigating the electroluminescence (EL) properties, the charge mobilities have been estimated by fabricating hole-only and electron-only devices (HODs and EODs), Figure S43. Under low bias, the curves were fitted in the space-charge-limited current (SCLC) region. Interestingly, as the size of the substituent increases, the charge mobility also shows a gradual augmentation. Remarkably, 1-mtp-SBF presents an excellent charge balance with considerably high mobility of 33.52×10^{-6} (hole) and 16.79×10^{-6} (electron) $cm^2V^{-1}s^{-1}$ for a material constructed on a SBF scaffold (3D shape). It is well established nowadays that a good balance between electron and hole flow is at least as important as the mobility values themselves to reach high PhOLED performances.[22,32] This ambipolarity is crucial for the device efficiency to ensure efficient recombination of hole and electron and is one reason for the excellent efficiency reported below. 1-p-SBF and 1-mbp-SBF also present a relatively good balance between hole and electron mobility, $0.64/0.42\times10^{-6}$ $cm^2V^{-1}s^{-1}$ for 1-p-SBF and $8.80/2.06\times10^{-6}$ $cm^2V^{-1}s^{-1}$ for 1-mbp-SBF though the values appear to be significantly lower than those of 1-mtp-SBF, emphasizing the chief role played by the pending substituent on the charge transport properties. Two important conclusions can be drawn. Firstly, the size of the substituent significantly improves the charge transport. This feature, which is a key point toward high PhOLED performance, is unravelled below thanks to the calculations of charge transfer integrals. Secondly, the three compounds present a good charge balance owing to the similar hole and electron mobilities. This behaviour can be, at least partially, assigned to the PHC nature of these hosts. Indeed, with heteroatom-based hosts, it is inherently difficult to balance the charge transport, due to the intrinsic properties of the constituting functional units (for example phosphine oxide or dicyanovinylene are efficient electron-transporting fragments, and it is often difficult to well balance their strong electron affinity).[32,59]

Based on theoretical considerations deduced from the crystalline structures of the three compounds, we will now discuss the possible origin of the fact that the hole and electron mobilities are significantly larger for 1-mtp-SBF. Whatever the charge transport model adopted (with the hopping and band regime as extreme cases), the transfer integrals (i.e. the electronic coupling) play a major role in dictating the charge mobility values. They are defined as $t_{ab} = <\psi_a|h|\psi_b>$, where ψ_a and ψ_b are the electronic wave functions of the HOMO/LUMO on neighbouring molecules a and b, respectively, and h is the one-electron Hamiltonian. Therefore, a simple way to assess charge transport performance is to compute and compare the transfer integrals in each system. We have computed such parameters for all direct neighbours in the crystal structures of 1-p-SBF, 1-mbp-SBF, and 1-mtp-SBF using a fragment method with Density Functional Theory (DFT) calculations at the B3LYP/DZ level using the ADF package.[60] The 1-p-SBF crystal consists of two different columnar stacks in the bc plane, alternating along the b axis, as highlighted by yellow and blue planes in Figure 4. Although quite heterogeneous, some transfer integrals are relatively high (especially considering the 3D shape of these materials) in the bc plane reaching values of 80 meV and 60 meV for the HOMO and LUMO, respectively. Hole transport is globally favoured in this system, especially along the a-axis, with a higher probability for the hole to move through the column highlighted in yellow (see right structure in Figure 4a). Transport in the 1-mtp-SBF crystal is confined to two dimensions with a homogeneous distribution of the transfer integrals, whether considering holes and electrons (Figure 4b). The transport network consists of two molecular sublayers in the bc plane (blue and yellow) stacked upon each other along the a-axis. Both sublayers display the same transfer integrals for holes and electrons. There is a preferential direction for transport within a layer (along the c axis) and in between the layers (along the a-axis).

Considering a layer of 1-mbp-SBF in the plane bc, electron transport has some 2D character, while hole transport only has 1D character (Figure 4c). Other relatively high transfer integrals can be found along the a-axis along which electrons and holes propagate in a rather equal manner. Overall, electrons travel in a three-dimensional space while holes are confined to two dimensions.

Judging solely by the analysis of the transfer integral amplitudes, one might predict 1-mbp-SBF or 1-p-SBF to be the best performing materials, in contrast with the experimental measurements (above). If we consider a simple hopping regime, the charge moves from one molecular site to another with a hopping rate given by Equation (1):[61]

$$k_{ET} = \frac{\pi |t_{ab}|^2}{\hbar \sqrt{\pi \lambda k_B T}} e^{-\frac{(\Delta G^\circ + \lambda)^2}{4 \lambda k_B T}} \quad (1)$$

where t_{ab} is the transfer integral between site a and site b, λ is the reorganization energy and ΔG° is the Gibbs free energy difference between the two sites (mostly induced by a voltage applied through the molecular crystal). From this equation, the higher the transfer integral, the higher the chance for the charge to hop between sites could be. Now, let us assume that a hypothetical hole is lying on one of the dimers associated with an electronic coupling at 83 meV in 1-p-SBF (Figure 4a) and that the thermal noise is not smoothing too much the diversity of transfer integrals at room temperature. In such a case, the charge will switch back and forth between the two molecules, causing it to stagnate and hence lowering the mobility. This is consistent with the transient localization model suggesting that the homogeneity of the transfer integrals is a key ingredient to promote high mobility values (the other being the relative sign of the transfer integrals that cannot be readily accessed

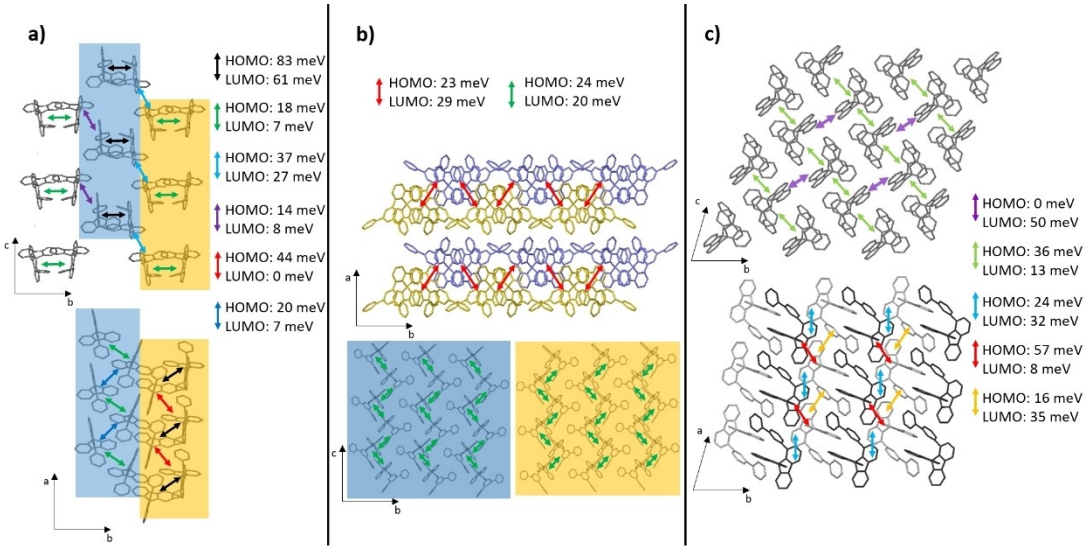

Figure 4. HOMO and LUMO transfer integral spatial distribution in the equilibrium structure of 1-p-SBF crystal (a), 1-mtp-SBF crystal (b) and 1-mbp-SBF crystal (c). Transfer integral values below 10 meV are not shown.

when the inequivalent molecules have different geometries in the unit cell, as it is the case here). This is further supported by the hole mobility data in a wide range of crystalline motifs for tetrathiafulvalene derivatives showing that the presence of a strongly interacting dimer (i.e. in a sandwiched herringbone structure) provides very low mobility values.[62] Note that the same argument applies for electron transport for a charge located in the dimer associated with the electronic coupling of 61 meV. Similarly, in 1-mbp-SBF, there is a strong inhomogeneity in the amplitude of the electronic couplings allowing for hole transport along the a direction (see blue and yellow arrows versus red ones). A similar dispersity also prevails for electron transport. This is less likely to happen in 1-mtp-SBF where the transfer integrals are much closer together (Figure 4b). In line with the transient localization model, we thus speculate that the homogeneity of the transfer integrals in 1-mtp-SBF is the key characteristic that enables efficient charge transport although it has overall lower values in comparison with the other two materials.

Finally, the three compounds were, first, incorporated as hosts for blue PhOLEDs. The phosphorescent emitter FIrpic was utilized as a blue emitter for devices B1, B2, and B3, in which 1-p-SBF, 1-mbp-SBF, and 1-mtp-SBF were respectively employed as hosts. Optimized blue PhOLEDs with architectures based on ITO/1,4,5,8,9,11-hexaazatriphenylenehexacarbonitrile (HAT-CN) (10 nm)/ 1,1-bis[(di-4-tolylamino)phenyl]cyclohexane (TAPC) (40 nm)/ 4,4′,4″-tris-(carbazol-9-yl)-triphenylamine (TCTA) (10 nm)/1,3-bis-(*N*-carbazolyl)benzene (mCP) (10 nm)/host: FIrpic (15 wt %, 20 nm)/ 1,3,5-tri[(3-pyridyl)-phen-3-yl]benzene (TmPyPB) (40 nm)/8-hydroxyquinolinolato-lithium (Liq) (2 nm)/Al (120 nm) were fabricated (Figure S44). HAT-CN/Liq were the hole/electron-injecting layer, TAPC/TmPyPB were the hole/electron-transporting layer, TCTA and mCP were both exciton-blocking layers. In the emitting layer (EML), the deep energy gap of the three PHC host materials from LUMO (≈−1.81/−1.88 eV) to HOMO (≈−5.93/−5.94 eV) can completely wrap the frontier electronic levels of the blue emitter (in identical experimental conditions, the HOMO/LUMO of FIrpic have been recently evaluated at −5.55 eV/−2.52 eV[32]). The detailed device performances are summarized in Table 2. As depicted in Figure 5, devices B1-B3 display a blue-light emission at 472 nm with corresponding Commission Internationale de l'Éclairage (CIE) coordinates of (0.14, 0.32), (0.14, 0.33) and

Table 2: Summary of devices performance of 1-p-SBF, 1-mbp-SBF and 1-mtp-SBF.

Device		Host	V_{on}[a] (V)	CE[b] (cd/A)	PE[b] (lm/W)	EQE[b] (%)	λ_{max}[c] (nm)	CIE (x, y)[c]
Blue	B1	**1-p-SBF**	3.6	40.0/37.5/32.8	34.5/27.6/19.4	21.0/19.7/17.3	472	(0.14, 0.32)
	B2	**1-mbp-SBF**	3.5	47.5/44.5/39.3	39.5/33.6/23.7	24.0/22.5/19.9	472	(0.14, 0.33)
	B3	**1-mtp-SBF**	3.5	50.0/47.0/42.3	44.6/35.1/26.1	25.6/24.1/21.7	472	(0.14, 0.32)
White	W1	**1-p-SBF**	3.3	73.3/69.3/63.1	66.6/58.6/45.2	24.5/23.6/21.4	556	(0.42,0.47)
	W2	**1-mbp-SBF**	3.3	75.0/70.7/65.2	67.9/59.5/47.3	25.3/24.2/22.3	556	(0.42, 0.47)
	W3	**1-mtp-SBF**	3.3	82.0/78.7/71.7	75.9/66.4/53.9	27.7/26.6/24.2	556	(0.42, 0.47)

[a] The operating voltage at onset. [b] Values of CE, PE, and EQE at the maximum, 100 cd m^{-2} and 1000 cd m^{-2}. [c] Measured at a driving current density of 5 mA cm^{-2}.

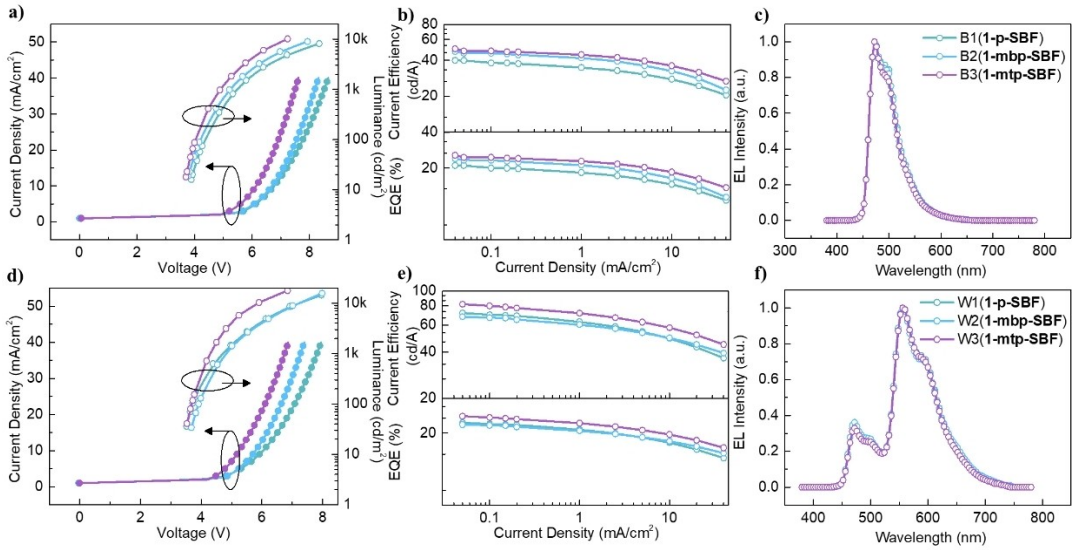

Figure 5. Device performance and EL spectra (at 5 mA cm^{-2}) of blue (a)–(c) and white (d)–(f) PhOLEDs using 1-p-SBF, 1-mbp-SBF and 1-mtp-SBF as host, respectively.

(0.14, 0.32), respectively. The turn-on voltages (V_{on}) were all detected to be very low, 3.6, 3.5 and 3.5 V for devices B1–B3 respectively, thus reflecting an excellent charge injection. Comparatively, device B3 using the host material 1-mtp -SBF successfully achieves the highest device efficiency with a maximum EQE (EQE_{max}) of 25.6 %, a maximum current efficiency (CE_{max}) of 50.0 cd A^{-1} and a maximum power efficiency (PE_{max}) of 44.6 lm W^{-1}. This exceeds the 25 % EQE threshold for the first time when using a PHC host in FIrpic-based blue PhOLEDs. Strikingly, with increasing current density, EQE of 21.7 % can be acquired under 1000 cd m^{-2}, which points to low-efficiency roll-off and excellent ability of carrier balance. In addition, devices B1 and B2 based on 1-p-SBF and 1-mbp-SBF, respectively, display very good device performance (B1: EQE_{max} = 21.0 %, CE_{max} = 40.0 cd A^{-1}, PE_{max} = 34.5 lm W^{-1}; B2: EQE_{max} = 24.0 %, CE_{max} = 47.5 cd A^{-1}, PE_{max} = 39.5 lm W^{-1}), showing the efficiency of the whole PHC concept and not of a single molecule. However, under 1000 cd m^{-2}, both devices B1 and B2 cannot maintain EQEs over 20 %, which is a little inferior to the values reached with device B3. Owing to the enhanced carrier-transport capacity, device B3 demonstrates higher brightness and stability than others under high operating voltage. At the molecular level, this shows the importance of the pending substituent in the device performance.

To interpret the very high performance obtained in this series, the phosphorescence lifetimes of the EMLs were investigated (Figure S45). The EMLs were exactly those used in the above-mentionned PhOLEDs (15 wt % FIrpic) and display lifetimes of 1.26, 1.31 and 1.29 μs for 1-mtp-SBF, 1-mbp-SBF, and 1-p-SBF, respectively. Thus, the lifetime of the EML using 1-mtp-SBF is shorter than those of 1-mbp-SBF and 1-p-SBF, which might help to reduce the triplet density and the possibility of triplet–triplet annihilation (TTA).[63–67] This feature is surely involved in the very high device performance obtained. Therefore, the excellent blue PhOLED performance reached with 1-mtp-SBF can be assigned to the combination of high E_{T1}, well-balanced mobility, and short deactivation lifetime.

To further explore the potential of PHC host materials for future lighting applications, the fabrication of white PhOLEDs is highly desirable. Device configurations with one single emitting layer white PhOLEDs were realized as: ITO/HAT-CN (10 nm)/TAPC (40 nm)/TCTA (10 nm)/mCP (10 nm)/host: FIrpic: PO-01 (1: 15 wt %: x wt %, 20 nm)/ 1,3,5-tris(6-(3-(pyridin-3-yl)phenyl)pyridin-2-yl)benzene (Tm3PyP26PyB) (45 nm)/Liq (2 nm)/Al (120 nm), as depicted in Figure S44. Based on the better charge balance and transfer shown in Figure S46, Tm3PyP26PyB appears to be more efficient as electron-transporting material than TmPyPB to achieve lower device consumption and higher power efficiency. In white PhOLEDs technology, these parameters are of great importance for low consumption and efficient lighting. In this device, a single EML, incorporating sky-blue and yellow phosphorescent emitters, is used and strongly contributes to the simplification of the device architecture compared to multi-layered RGB EML. The detailed EL characteristics of the devices are summarized in Figure S47 and Table S21 when changing the doping ratios x of PO-01 from 0.25 wt % to 1.5 wt % while keeping FIrpic at 15 wt %. The optimized white devices based on the three PHC host materials are obtained with an optimal doping ratio of x = 0.5 wt % for PO-01. As shown in Figure 5, devices W1-3 respectively based on 1-p-SBF, 1-mbp-SBF, and 1-mtp-SBF all exhibit a warm white light emission with CIE coordinates of (0.42, 0.47). Device W3 achieved remarkable performance with CE_{max} of 82.0 cd A^{-1}, PE_{max} of 75.9 lm W^{-1}, and EQE_{max} of 27.7 % under a low turn-on voltage of 3.3 V, which is a breakthrough result in white PhOLEDs based on PHC host materials. It should be noted that an ultra-low efficiency roll-off was accomplished at 1000 cd m^{-2} with device W3, which displays high efficiencies of 71.7 cd A^{-1}, 53.9 lm W^{-1}, and 24.2 %. Nevertheless, devices W1 and W2 with the same turn-on voltage of 3.3 V also achieve good device efficiencies (W1: CE_{max} = 73.3 cd A^{-1}, PE_{max} = 66.6 lm W^{-1} and EQE_{max} = 24.5 %, W2: CE_{max} = 75.0 cd A^{-1}, PE_{max} = 67.9 lm W^{-1} and EQE_{max} = 25.3 %) confirming, as evidenced above in the case of blue PhOLEDs, the efficiency of the whole approach and not of a single molecule. Table S22 depicts the most efficient white PhOLEDs reported to date in the literature, showing that only a few of them can achieve high EQEs over 25 %. Thus, the present PHC-based white PhOLEDs display similar efficiencies as the best reported to date with heteroatom-based hosts and highlight the real potential of this novel molecular design strategy for the future of white PhOLEDs.

Conclusion

In summary, we report a new molecular design of high-efficiency hosts based on the association of simple benzene units for white PhOLEDs. These spiro-configured hosts are extremely simple in their structure and easy to synthesize in a short and highly efficient manner. By exploiting the C1 position of the SBF scaffold, a sterically hindered environment is obtained, providing excellent photophysical properties, a large HOMO/LUMO gap, and a high E_{T1}. Of particular interest, the charge transport properties are drastically modified by the substituent but remain, in all cases, always well-balanced, which is an important asset in this technology. The charge transport properties have been rationalized by theoretical calculations showing the importance of the homogeneity of charge transfer integrals in mobility values. When incorporating the hosts in blue and white PhOLEDs, which are the most challenging nowadays, excellent performances were obtained. In particular, 1-mtp-SBF achieves the best results with EQEs of 25.6 % in blue and 27.7 % in white PhOLEDs. The performance of FIrpic-based blue PhOLEDs is the highest reported to date for PHCs. The performance of white PhOLEDs compete with the best reported to date in the literature using traditional heteroatom-based hosts and show that the PHC strategy should now be carefully considered for the next generation of host materials.[68] This work proves that PHCs can act as excellent hosts for the new generation of white PhOLEDs

for lighting applications and pave the way for the development of a simpler large-scale electronics.

Experimental Details can be found in Supporting Information.

Acknowledgements

We thank the National Natural Science Foundation of China (grant Nos. 51873139, 61961160731, 62175171 and 22175124) and Suzhou Science and Technology Plan Project (SYG202010) for funding. We thank the CDFIX and CRMPO (Rennes), GENCI (N°AD0100805032R1) for computing time, the ANR (Project SpiroQuest N°19-CE05-0024) and the ADEME (Ecoelec Project) for PhD grant (CB respectively). This work has also been supported by Suzhou Key Laboratory of Functional Nano & Soft Materials, Collaborative Innovation Center of Suzhou Nano Science & Technology, the 111 Project, Joint International Research Laboratory of Carbon-Based Functional Materials and Devices. The work in Mons has been supported by the Marie Curie ITN project UHMob (GA-811284) and the Consortium des Équipements de Calcul Intensif (CÉCI), funded by the Fonds de la Recherche Scientifique de Belgique (F.R.S.-FNRS) under grant no. 2.5020.11. J.C. is an F.R.S.-FNRS research director.

Conflict of Interest

The authors declare no conflict of interest.

Data Availability Statement

The data that support the findings of this study are available from the corresponding author upon reasonable request.

Keywords: Blue Emission · Host Materials · Organic Electronics · Phosphorescent Organic Light-Emitting Diodes · Pure Aromatic Hydrocarbons · White Emission

[1] G. Hong, X. Gan, C. Leonhardt, Z. Zhang, J. Seibert, J. M. Busch, S. Bräse, *Adv. Mater.* **2021**, *33*, 2005630.
[2] C. Poriel, J. Rault-Berthelot, *Adv. Funct. Mater.* **2020**, *30*, 1910040.
[3] J. R. Sheats, H. Antoniadis, M. Hueschen, W. Leonard, J. Miller, R. Moon, D. Roitman, A. Stocking, *Science* **1996**, *273*, 884–888.
[4] R. H. Friend, R. W. Gymer, A. B. Holmes, J. H. Burroughes, R. N. Marks, C. Taliani, D. D. C. Bradley, D. A. Dos Santos, J. L. Bredas, M. Lögdlund, W. R. Salaneck, *Nature* **1999**, *397*, 121–128.
[5] M. A. Baldo, D. F. O'Brien, Y. You, A. Shoustikov, S. Sibley, M. E. Thompson, S. R. Forrest, *Nature* **1998**, *395*, 151–154.
[6] Y. Tao, C. Yang, J. Qin, *Chem. Soc. Rev.* **2011**, *40*, 2943–2970.
[7] K. S. Yook, J. Y. Lee, *Adv. Mater.* **2014**, *26*, 4218–4233.
[8] C. Poriel, J. Rault-Berthelot, *J. Mater. Chem. C* **2017**, *5*, 3869–3897.
[9] C. Poriel, J. Rault-Berthelot, *Adv. Funct. Mater.* **2021**, *31*, 2010547.
[10] Q. Wang, F. Lucas, C. Quinton, Y.-K. Qu, J. Rault-Berthelot, O. Jeannin, S.-Y. Yang, F.-C. Kong, S. Kumar, L.-S. Liao, C. Poriel, Z.-Q. Jiang, *Chem. Sci.* **2020**, *11*, 4887–4894.
[11] Y. Wang, J. H. Yun, L. Wang, J. Y. Lee, *Adv. Funct. Mater.* **2021**, *31*, 2008332.
[12] A. Endo, M. Ogasawara, A. Takahashi, D. Yokoyama, Y. Kato, C. Adachi, *Adv. Mater.* **2009**, *21*, 4802–4806.
[13] M. Y. Wong, E. Zysman-Colman, *Adv. Mater.* **2017**, *29*, 1605444.
[14] Z. Cai, X. Wu, H. Liu, J. Guo, D. Yang, D. Ma, Z. Zhao, B. Z. Tang, *Angew. Chem. Int. Ed.* **2021**, *60*, 23635–23640; *Angew. Chem.* **2021**, *133*, 23827–23832.
[15] K.-T. Wong, Y.-L. Liao, Y.-T. Lin, H.-C. Su, C.-C. Wu, *Org. Lett.* **2005**, *7*, 5131–5134.
[16] J. Ma, M. Idris, T. Y. Li, D. S. M. Ravinson, T. Fleetham, J. Kim, P. I. Djurovich, S. R. Forrest, M. E. Thompson, *Adv. Opt. Mater.* **2022**, *10*, 2101530.
[17] L. J. Sicard, H.-C. Li, Q. Wang, X.-Y. Liu, O. Jeannin, J. Rault-Berthelot, L.-S. Liao, Z.-Q. Jiang, C. Poriel, *Angew. Chem. Int. Ed.* **2019**, *58*, 3848–3853; *Angew. Chem.* **2019**, *131*, 3888–3893.
[18] C. Poriel, J. Rault-Berthelot, *Acc. Mater. Res.* **2022**, *3*, 379–390.
[19] M. Zhuo, W. Sun, G. Liu, J. Wang, L. Guo, C. Liu, B. Mi, J. Song, Z. Gao, *J. Mater. Chem. C* **2015**, *3*, 9137–9144.
[20] G. Tian, Y. Jiang, P. Wu, J. Huang, Q. Zou, Q. Wang, H. Mu, J. Su, *New J. Chem.* **2016**, *40*, 9500–9506.
[21] Y. Luo, Z. Liu, G. Yang, T. Wang, Z. Bin, J. Lan, D. Wu, J. You, *Angew. Chem. Int. Ed.* **2021**, *60*, 18852–18859; *Angew. Chem.* **2021**, *133*, 19000–19007.
[22] A. Yoshii, Y. Onaka, K. Ikemoto, T. Izumi, S. Sato, H. Kita, H. Taka, H. Isobe, *Chem. Asian J.* **2020**, *15*, 2181–2186.
[23] D. Y. Kondakov, W. C. Lenhart, W. F. Nichols, *J. Appl. Phys.* **2007**, *101*, 024512.
[24] N. Lin, J. Qiao, L. Duan, H. Li, L. Wang, Y. Qiu, *J. Phys. Chem. C* **2012**, *116*, 19451–19457.
[25] N. Lin, J. Qiao, L. Duan, L. Wang, Y. Qiu, *J. Phys. Chem. C* **2014**, *118*, 7569–7578.
[26] H. Li, M. Hong, A. Scarpaci, X. He, C. Risko, J. S. Sears, S. Barlow, P. Winget, S. R. Marder, D. Kim, J.-L. Brédas, *Chem. Mater.* **2019**, *31*, 1507–1519.
[27] J.-H. Lee, C.-H. Chen, P.-H. Lee, H.-Y. Lin, M.-k. Leung, T.-L. Chiu, C.-F. Lin, *J. Mater. Chem. C* **2019**, *7*, 5874–5888.
[28] D. Li, J. Li, D. Liu, W. Li, C.-L. Ko, W.-Y. Hung, C. Duan, *ACS Appl. Mater. Interfaces* **2021**, *13*, 13459–13469.
[29] Q.-L. Xu, X. Liang, S. Zhang, Y.-M. Jing, X. Liu, G.-Z. Lu, Y.-X. Zheng, J.-L. Zuo, *J. Mater. Chem. C* **2015**, *3*, 3694–3701.
[30] W. Song, Q. Xu, J. Zhu, Y. Chen, H. Mu, J. Huang, J. Su, *ACS Appl. Mater. Interfaces* **2020**, *12*, 19701–19709.
[31] X. Tang, X.-Y. Liu, Y. Yuan, Y.-J. Wang, H.-C. Li, Z.-Q. Jiang, L.-S. Liao, *ACS Appl. Mater. Interfaces* **2018**, *10*, 29840–29847.
[32] F. Lucas, C. Quinton, S. Fall, T. Heiser, D. Tondelier, B. Geffroy, N. Leclerc, J. Rault-Berthelot, C. Poriel, *J. Mater. Chem. C* **2020**, *8*, 16354–16367.
[33] W.-C. Chen, Y. Yuan, Z.-L. Zhu, Z.-Q. Jiang, S.-J. Su, L.-S. Liao, C.-S. Lee, *Chem. Sci.* **2018**, *9*, 4062–4070.
[34] K. Udagawa, H. Sasabe, C. Cai, J. Kido, *Adv. Mater.* **2014**, *26*, 5062–5066.
[35] T. P. I. Saragi, T. Spehr, A. Siebert, T. Fuhrmann-Lieker, J. Salbeck, *Chem. Rev.* **2007**, *107*, 1011–1065.
[36] Y.-K. Qu, Q. Zheng, J. Fan, L.-S. Liao, Z.-Q. Jiang, *Acc. Mater. Res.* **2021**, *2*, 1261–1271.
[37] C. Poriel, L. Sicard, J. Rault-Berthelot, *Chem. Commun.* **2019**, *55*, 14238–14254.
[38] R. Pudzich, T. Fuhrmann-Lieker, J. Salbeck, *Adv. Polym. Sci.* **2006**, *199*, 83–142.

[39] L.-H. Xie, J. Liang, J. Song, C.-R. Yin, W. Huang, *Curr. Org. Chem.* **2010**, *14*, 2169–2195.
[40] S. Liu, D. Xia, M. Baumgarten, *ChemPlusChem* **2021**, *86*, 36–48.
[41] M. Zhu, C. Yang, *Chem. Soc. Rev.* **2013**, *42*, 4963–4976.
[42] L. Sicard, C. Quinton, J.-D. Peltier, D. Tondelier, B. Geffroy, U. Biapo, R. Métivier, O. Jeannin, J. Rault-Berthelot, C. Poriel, *Chem. Eur. J.* **2017**, *23*, 7719–7723.
[43] C. Poriel, C. Quinton, F. Lucas, J. Rault-Berthelot, Z. Q. Jiang, O. Jeannin, *Adv. Funct. Mater.* **2021**, *31*, 2104980.
[44] J. Zhao, S. Yuan, X. Du, W. Li, C. Zheng, S. Tao, X. Zhang, *Adv. Opt. Mater.* **2018**, *6*, 1800825.
[45] Q. Wang, J. Ding, D. Ma, Y. Cheng, L. Wang, X. Jing, F. Wang, *Adv. Funct. Mater.* **2009**, *19*, 84–95.
[46] H. Huang, X. Yang, Y. Wang, B. Pan, L. Wang, J. Chen, D. Ma, C. Yang, *Org. Electron.* **2013**, *14*, 2573–2581.
[47] K. Gao, K. Liu, X.-L. Li, X. Cai, D. Chen, Z. Xu, Z. He, B. Li, Z. Qiao, D. Chen, Y. Cao, S.-J. Su, *J. Mater. Chem. C* **2017**, *5*, 10406–10416.
[48] L.-S. Cui, Y. Liu, X.-Y. Liu, Z.-Q. Jiang, L.-S. Liao, *ACS Appl. Mater. Interfaces* **2015**, *7*, 11007–11014.
[49] X. Tang, X.-Y. Liu, Z.-Q. Jiang, L.-S. Liao, *Adv. Funct. Mater.* **2019**, *29*, 1807541.
[50] B. W. D'Andrade, R. J. Holmes, S. R. Forrest, *Adv. Mater.* **2004**, *16*, 624–628.
[51] X.-K. Liu, C.-J. Zheng, M.-F. Lo, J. Xiao, Z. Chen, C.-L. Liu, C.-S. Lee, M.-K. Fung, X.-H. Zhang, *Chem. Mater.* **2013**, *25*, 4454–4459.
[52] B. Zhang, G. Tan, C.-S. Lam, B. Yao, C.-L. Ho, L. Liu, Z. Xie, W.-Y. Wong, J. Ding, L. Wang, *Adv. Mater.* **2012**, *24*, 1873–1877.
[53] Y. Zhao, C. Wu, P. Qiu, X. Li, Q. Wang, J. Chen, D. Ma, *ACS Appl. Mater. Interfaces* **2016**, *8*, 2635–2643.
[54] L. Sicard, C. Quinton, F. Lucas, O. Jeannin, J. Rault-Berthelot, C. Poriel, *J. Phys. Chem. C* **2019**, *123*, 19094–19104.
[55] Deposition Numbers 2142857 (**1-mtp-SBF**), 2168574 (for **1-mbp-SBF**), and 1495896 (for **1-p-SBF**) contains the supplementary crystallographic data for this paper. These data are provided free of charge by the joint Cambridge Crystallographic Data Centre and Fachinformationszentrum Karlsruhe Access Structures service.
[56] S. Thiery, C. Declairieux, D. Tondelier, G. Seo, B. Geffroy, O. Jeannin, R. Métivier, J. Rault-Berthelot, C. Poriel, *Tetrahedron* **2014**, *70*, 6337–6351.
[57] C. Poriel, Y. Ferrand, P. Le Maux, J. Rault-Berthelot, G. Simonneaux, *Inorg. Chem.* **2004**, *43*, 5086–5095.
[58] C. Poriel, Y. Ferrand, P. Le Maux, C. Paul-Roth, G. Simonneaux, J. Rault-Berthelot, *J. Electroanal. Chem.* **2005**, *583*, 92–103.
[59] J.-D. Peltier, B. Heinrich, B. Donnio, E. Jacques, J. Rault-Berthelot, C. Poriel, *ACS Appl. Mater. Interfaces* **2017**, *9*, 8219–8232.
[60] K. Senthilkumar, F. C. Grozema, F. M. Bickelhaupt, L. D. A. Siebbeles, *J. Chem. Phys.* **2003**, *119*, 9809–9817.
[61] S. Chaudhuri, S. Hedström, D. D. Méndez-Hernández, H. P. Hendrickson, K. A. Jung, J. Ho, V. S. Batista, *J. Chem. Theory Comput.* **2017**, *13*, 6000–6009.
[62] M. Mas-Torrent, P. Hadley, S. T. Bromley, X. Ribas, J. Tarrés, M. Mas, E. Molins, J. Veciana, C. Rovira, *J. Am. Chem. Soc.* **2004**, *126*, 8546–8553.
[63] A. Köhler, H. Bässler, *Mater. Sci. Eng.* **2009**, *66*, 71–109.
[64] F. Steiner, J. Vogelsang, J. M. Lupton, *Phys. Rev. Lett.* **2014**, *112*, 137402.
[65] M. A. Baldo, C. Adachi, S. R. Forrest, *Phys. Rev. B* **2000**, *62*, 10967–10977.
[66] Y.-K. Wang, Q. Sun, S.-F. Wu, Y. Yuan, Q. Li, Z.-Q. Jiang, M.-K. Fung, L.-S. Liao, *Adv. Funct. Mater.* **2016**, *26*, 7929–7936.
[67] Q. Wang, Q.-S. Tian, Y.-L. Zhang, X. Tang, L.-S. Liao, *J. Mater. Chem. C* **2019**, *7*, 11329–11360.
[68] C. Poriel, J. Rault-Berthelot, Z.-Q. Jiang, *Mater. Chem. Front.* **2022**, *6*, 1246-1252.

Manuscript received: May 17, 2022
Accepted manuscript online: June 21, 2022
Version of record online: July 14, 2022